University of South Bohemia in České Budějovice

Faculty of Science

Functional assignment for the N-terminal segments of cyanobacterial Hli proteins

Bachelor thesis

Václav Vincik

Supervisor: **Doc. Ing. Roman Sobotka, Ph.D.**

Institute of Microbiology, Academy of Sciences of the Czech Republic

Třeboň, and University of South Bohemia, České Budějovice

České Budějovice 2023

This thesis should be cited as:

Vincik, V., 2023: Functional assignment for the N-terminal segments of cyanobacterial Hli proteins. Bachelor Thesis. University of South Bohemia, Faculty of Science, České Budějovice, Czech Republic, 41 p.

Annotation

Light harvesting antennas (LHC) of green algae and plants are unique in their ability to alternate between light harvesting, where absorbed energy is transferred to photosystems, and photoprotection, where this energy is dissipated as heat. This thesis examines their cyanobacterial ancestors, the High light-inducible proteins (Hlips). The model cyanobacterium, *Synechocystis* PCC 6803, contains a set of four Hlips (HliA-D) that bind two different pigments (chlorophyll and β-carotene), form a specific set of homo- and heterodimers, and, finally, recognize other protein partners (Ycf39, Chl-synthase, CP47). However, the mechanism of how Hlips recognize their protein partners is unclear. This thesis aims to clarify the importance of the Hlip-specific N-terminus and the highly conserved transmembrane helix in preventing homo-dimerization of HliA and HliB and binding PSII-assembly-related protein. According to a recent hypothesis, the N-terminus is solely responsible for recognizing PSII factors and subunits, while the membrane helix determines the specificity of Hlip-Hlip interactions. To address this model, *Synechocystis* strains producing chimeric Hlips were synthesized, each fusing the N-terminal domain from one Hlip with the transmembrane helix from another, followed by their purification and characterization of the interaction with other proteins and pigments.

Declaration [in Czech]

Prohlašuji, že jsem autorem této kvalifikační práce a že jsem ji vypracoval pouze s použitím pramenů literatury uvedených v seznamu použitých zdrojů.

České Budějovice, 1.12. 2023 Václav Vincik

Acknowledgments

I would like to express my profound gratitude to my supervisors, Minna Koskela, Ph.D., and especially to doc. Ing. Roman Sobotka, Ph.D., for their invaluable guidance, patience, and unwavering support throughout my research journey. Their insights and expertise have been pivotal in shaping my work. Special thanks are also due to Lucia Kovářová and Anna Wysocka for mentoring me. They were always available to offer help and advice. I extend my appreciation to the entire group of doc. Sobotka and the group of Prof. Komenda, their collective wisdom has been a constant source of inspiration. On a deeply personal note, I wish to express my eternal gratitude to my beloved mother. Her passing before the completion of this work leaves a void. I dedicate this work to her memory. Lastly, my sincere thanks go to my close friends, whose unwavering support and encouragement have been invaluable throughout this journey. This thesis would not have been possible without the contributions and support of all these individuals, and I am deeply thankful for their involvement in my academic endeavor.

TABLE OF CONTENTS

INTRODUCTION

Significance of photosynthesis

Photosynthesis is a fundamental biochemical process that converts solar energy into chemical energy through light absorption, energy transduction, and carbon fixation (Verméglio, 2001). It involves light absorption by pigment chromatophores, light-powered oxidation of various substrates by photosynthetic reaction center(s), and transfer of electrons through a series of reactions generating a proton gradient. Oxygenic photosynthesis is distinguished from anoxygenic photosynthesis (found in some bacteria) by utilizing chlorophyll (Chl) pigments with higher redox potential than bacteriochlorophyll, allowing water oxidization. Oxygen is released as a by-product of this type of photosynthesis. On a broader ecological scale, the primary production (synthesis of organic compounds from atmospheric or aquatic carbon dioxide) predominantly occurs through the process of oxygenic photosynthesis, where the activity of photoautotrophic organisms such as plants, algae, and cyanobacteria fuels food webs, influences climate patterns, and even drives biogeochemical cycles (Field *et al.*, 1998).

From an evolutionary standpoint, the advent of oxygenic photosynthesis significantly impacted the planet's geochemistry. During the Proterozoic Eon, ~2.3 billion years, cyanobacteria, the first oxygenic phototrophs, played a crucial role in Earth's oxygenation (Sessions *et al.*, 2009). The rise of oxygenic photosynthesis led to a significant increase in atmospheric oxygen levels, which proposedly triggered a global climate disaster and potentially caused mass extinctions (Kopp *et al.*, 2005). However, it also altered the course of development of life on Earth in a rather positive way by allowing the emergence of aerobic life forms and multicellular life as we know it today (Soo *et al.*, 2017).

Biochemistry of photosynthesis

Photosynthesis can be categorized into two concomitant sets of reactions: the light-dependent and light-independent reactions, referred to as the Calvin-Benson cycle. (Nelson & Yocum, 2006). During light-dependent reactions, two complicated, light-powered oxidoreductases (Photosystem I and Photosystem II), together with other membrane complexes, generate ATP and produce redox power for the reduction of $NADP^+$ to NADPH. These molecules then serve

as the energy currency and reduce equivalents for downstream metabolic processes (Mitchell, 1961).

Concurrently, the Calvin-Benson cycle, a series of light-independent enzymatic reactions, operates to fix atmospheric carbon dioxide into organic molecules. This cycle involves three key phases: i) carbon fixation, where CO_2 is attached to ribulose-1,5-bisphosphate by the enzyme RuBisCO (ribulose-1,5-bisphosphate carboxylase/oxygenase); ii) reduction, where the fixed carbon is reduced using NADPH; iii) regeneration of the ribulose-1,5-bisphosphate. ATP and NADPH, also produced in the light-dependent reactions, provide the necessary energy for the process. The immediate product of the cycle is glyceraldehyde-3-phosphate, which serves as a precursor for various biosynthetic pathways. (Benson, 2002; Raines, 2003).

Importance of cyanobacteria for photosynthesis research

In the realm of oxygenic photosynthetic organisms, cyanobacteria offer an invaluable model system. They are the only group of bacteria that perform oxygenic photosynthesis, while other groups evolved different types of anoxygenic photosynthesis (Sánchez-Baracaldo & Cardona, 2019). They also serve as evolutionary precursors to plant chloroplasts, as postulated by endosymbiotic theory (Keeling, 2010; Kumar *et al.*, 2021). According to this theory, an ancestral photosynthetic prokaryote related to cyanobacteria was engulfed by a eukaryotic cell, leading to the establishment of a symbiotic relationship and the eventual evolution of chloroplasts (Sugiura *et al.*, 1998). The idea of cyanobacterial origin of chloroplast is supported by the fact that both perform oxygenic photosynthesis, share similar membrane structures (Westphal *et al.*, 2001), utilize the same type of photosynthetic pigment – Chl-*a*, and, according to phylogenetic analyses, share similarities in gene sequences (Sato, 2021; Vitha *et al.*, 2003).

Cyanobacteria and eukaryotic phototrophs (plants and algae) also use the same biosynthetic pathways of galactolipids (Yuzawa *et al.*, 2011), which are the main building blocks of the specialized internal membrane system – thylakoids (TM), which contain photosynthetic machinery. TM in cyanobacteria has a unique architecture (see Fig. 1). Electron tomography studies have shown that the TM network exhibits areas of quasi-helical arrangement, similar to the TM system found in chloroplasts, allowing for efficient light capture and energy transfer within the membrane (Liberton *et al.*, 2010).

One of the key photosynthetic complexes present in TM is Photosystem II (PSII; Fig. 1), already mentioned above. PSII is assembled from tens of proteins and various cofactors, which includes the oxygen-evolving complex (OEC) responsible for the photo-oxidization of water molecules. OEC is a cluster of manganese, calcium, and oxygen atoms. When PSII absorbs light, the energy is transferred to its reaction center, specifically to a pair of Chl molecules known as P680. The excitation of P680 leads to the transfer of an electron to a series of electron carriers, culminating in the reduction of plastoquinone to plastoquinol. This electron transfer is coupled with the extraction of electrons from water by the OEC, which produces molecular oxygen (O_2) as a byproduct (Barber, 2012). Furthermore, PSII is involved in the generation of ATP through a linear electron transfer (Dang *et al.*, 2014).

In addition to PSII, the TM contains other protein complexes involved in the electron transport chain and ATP synthesis. These include the cytochrome b_6f complex (Fig. 1), which transfers electrons between PSII and Photosystem I (PSI). The cytochrome b_6f is crucial in generating a proton gradient across the TM, essential for ATP synthesis. PSI absorbs light energy and transfers electrons to reduce ferredoxin, which is later used to reduce $NADP^+$ to NADPH to synthesize organic compounds. Furthermore, the ATP synthase complex is embedded in TM and synthesizes ATP using the proton gradient generated by the electron transport chain.

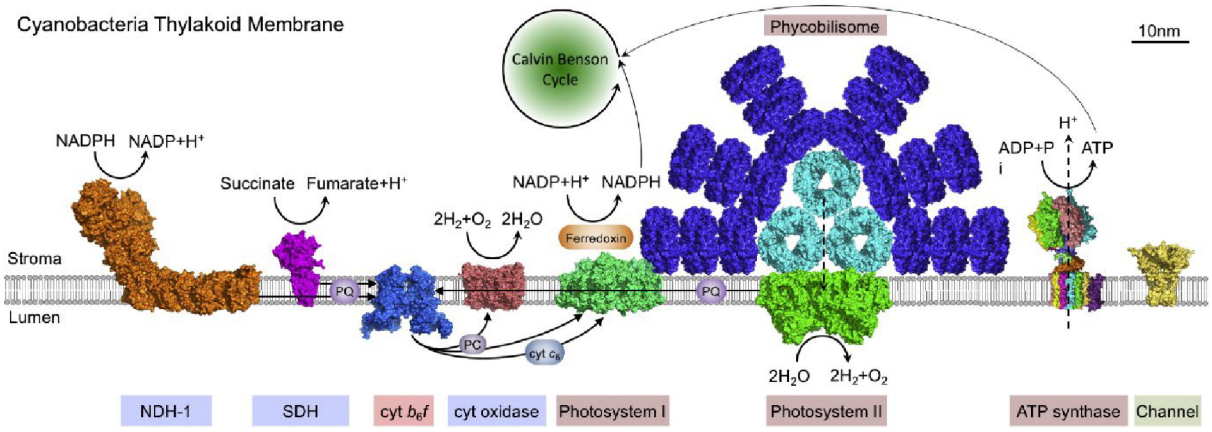

Fig. 1: Structural representation of the cyanobacterial TM. *Among the photosynthetic and respiratory electron transport complexes is the phycobilisome - a membrane-associated light-harvesting antenna that captures light energy and facilitates its transfer to PSII and PSI. Other complexes are cytochrome b_6f (cyt b_6f) and ATP synthase (ATPase). In addition to these macroscopic complexes, TM hosts a range of smaller electron transport molecules—plastoquinone (PQ), plastocyanin (PC), and cytochrome c_6. These molecular entities function as electron carriers and are instrumental in shuttling electrons between the various electron transport complexes. By doing so, they establish functional linkages among*

all the integral complexes, facilitating a flow of electrons within the photosynthetic apparatus (Liu, 2004).

Structure of photosystems

PSI and PSII are sophisticated molecular assemblies harboring an array of cofactors and protein subunits that function in tandem to enable photochemical reactions and subsequent electron transfer processes (Jordan *et al.*, 2001; Umena *et al.*, 2011). PSI is a protein-pigment complex primarily composed of two large PsaA and PsaB core subunits (see Fig. 2), as well as several smaller subunits. The primary function of PSI is to absorb light and drive the transfer of electrons from plastocyanin or cytochrome c_6 to ferredoxin. This process is facilitated by Chl-*a* molecules and a series of iron-sulfur clusters, integral to electron transfer mechanisms (Jordan *et al.*, 2001; Mazor *et al.*, 2017).

In contrast to PSI, the PSII complex consists of four large subunits. While structurally similar D1 and D2 proteins form the reaction center together, two additional core subunits, CP43 and CP47 (see Fig. 2 and 3), are closely associated and play a key role in binding Chl and other pigments, thus facilitating light absorption (Wei *et al.*, 2016).

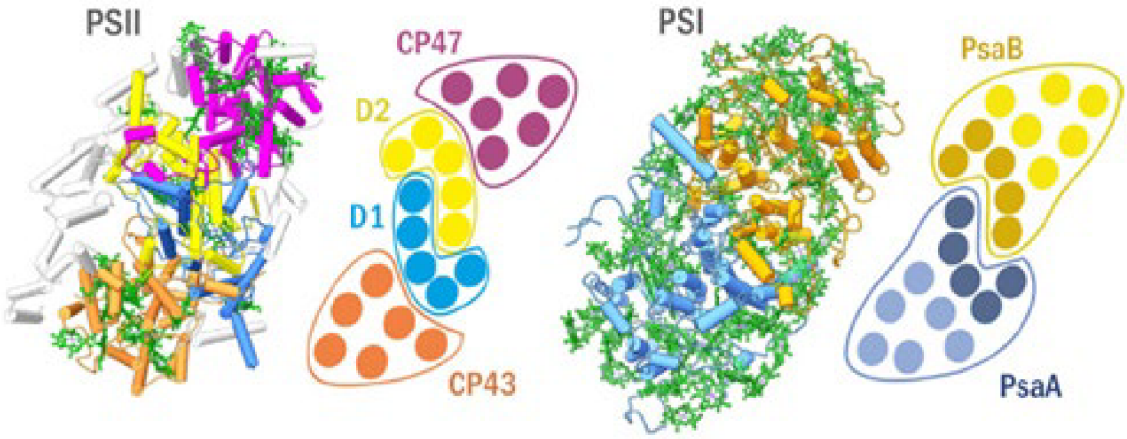

Fig. 2: A schema of the structure of photosystems. *PSII (left) and PSI (right) structure and schematic helical arrangement of their main Chl-binding proteins (D1 in blue, D2 in yellow, CP47 in violet, CP43 in brown; PsaA in blue with antenna helices in light blue, and PsaB in ochre with antenna helices in light ochre) (Komenda & Sobotka, 2019).*

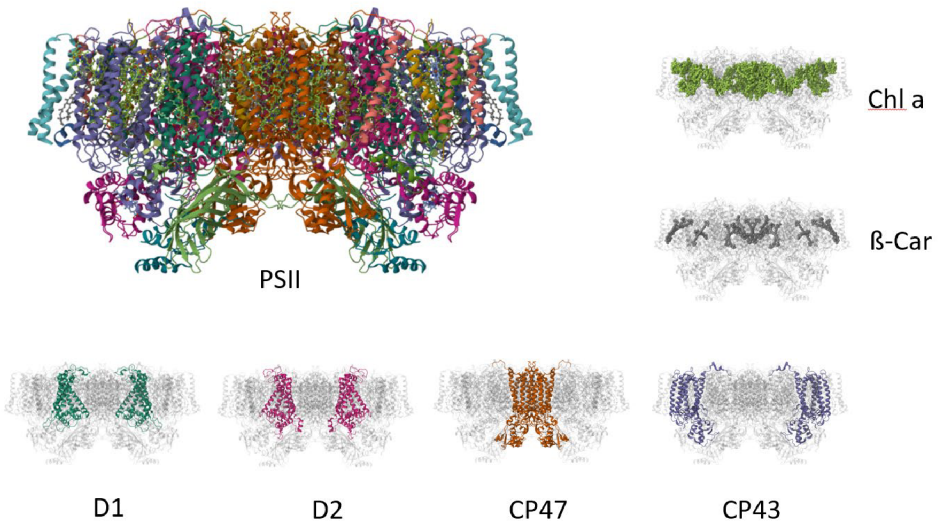

Fig. 3: Visual representation of the structure of dimeric PSII. *The complex is composed of multicolored protein subunits. Adjacent, individual proteins are highlighted: Chl (green), β-Car (dark grey), D1 protein (teel), D2 protein (pink), CP47 subunit (orange), CP43 subunit (blue). Based on the X-ray PSII structure with PDB code 2AXT (Loll et al., 2005).*

Light harvesting proteins in plants and cyanobacteria

In phototrophic organisms, the photosynthetic apparatus has evolved as a well-tuned system for the efficient absorption and conversion of light energy into chemical energy. To maximize this efficiency, peripheral light-harvesting complexes complement the core photosystems. External antennas expand the absorption capabilities and channel the absorbed energy toward the reaction centers located in the core photosystems. Additionally, antennas exhibit dynamic structural and functional modifications in response to environmental cues, particularly light quality and intensity (Engelken *et al.*, 2010).

Phycobilisomes, found in cyanobacteria and red algae, represent light-harvesting complexes associated with the TM and are composed of oligomeric phycobiliproteins that bind bilins (e.g., phycocyanin or phycoerythrin) as chromophores, as shown on Fig. 1 and Fig. 4. Absorbed energy (exciton) is transferred to Chl molecules in the photosynthetic reaction centers. The diversity of phycobiliproteins in a single phycobilisome allows light absorption across a broad range of wavelengths and, therefore, an efficient photon capture in environments with varying light conditions (Wilson *et al.*, 2006). Their function is thus similar to the antennas of plants (LHCs; Fig. 4), highlighting the evolutionary adaptations in different phototrophic organisms for maximizing light energy utilization.

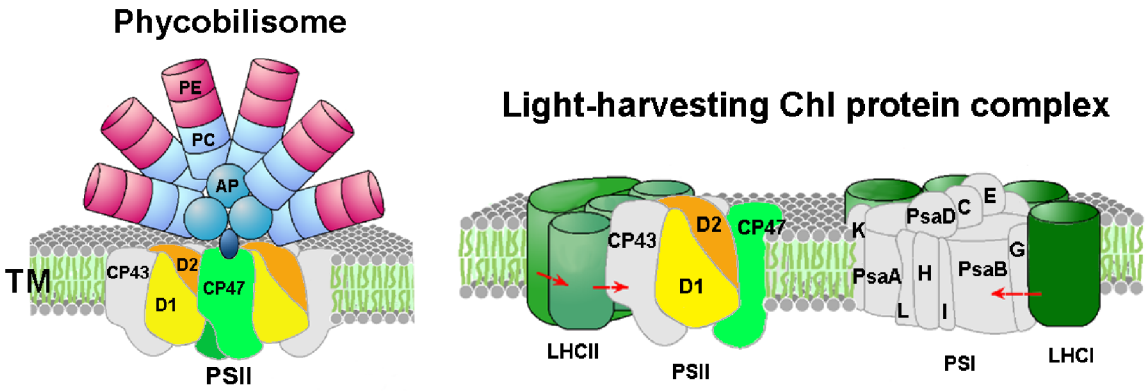

Fig. 4: Detailed representation of the photosynthetic antenna proteins. Left: *The phycobilisomes are found in cyanobacteria and red algae. At its core is the terminal pigment surrounded by layers of different pigment-protein complexes. Allophycocyanin (AP) is situated closest to the terminal pigment (blue), while phycocyanin (PC) / phycoerythrocyanin (PEC) is more peripheral (light blue). Phycoerythrin (PE) typically forms the most external layers (rods; pink). Light is absorbed by these pigments and directed toward PSII, represented by the D1 (yellow) and D2 (orange) protein complexes, along with CP43 (grey) and CP47 (bright green).* ***Right:*** *The light-harvesting Chl protein complex (LHCs) as found in plants and green algae. Two main complexes are LHCII, associated with PSII, depicted as an assembly of green cylinders. LHCI, which are tightly associated with PSI, are also depicted as a set of green cylinders, along with the core proteins PsaA to PsaB. Red arrows indicate the path of absorbed light energy as it is transferred to the reaction centers of PSII and PSI (Kanehisa Laboratories, modified.)*

High-light inducible proteins

Cyanobacterial high-light-inducible proteins (Hlips) are the evolutionary ancestors of light-harvesting antennae of plants and green algae. Hlips are single-helix, pigment-binding transmembrane proteins and are massively upregulated under various stress conditions, such as high light intensity, ultraviolet radiation, and nutrient deprivation (Dolganov *et al.*, 1995; He *et al.*, 2001). Initially recognized for their association with unassembled PSII subunits, Hlips play a critical role in protecting the PSII assembly process under stress (Havaux *et al.*, 2003; Komenda & Sobotka, 2016). Their photoprotective role is probably based on their ability to dissipate absorbed light energy through non-photochemical quenching mechanisms (Staleva *et al.*, 2015).

The binding of pigments by Hlips involves a highly-conserved ExxNxR motif, which is characteristic of the whole LHC protein superfamily, including Hlips, plant/algae light antennas, and various eukaryotic LHC-like proteins. (see Fig. 5). The ExxNxR motif is apparently involved in the binding of Chl molecules and the stabilization of two central helices in LHCs via an E-R salt bridge (Liu *et al.*, 2004). Indeed, the dimerization of Hlips appears

essential for the pigment binding and the ability to form an energy-dissipative configuration (Staleva *et al.*, 2015; Pazderník *et al.*, 2019). A proposed structure of a Hlip dimer associated with pigments is depicted in Fig. 5. Genomic sequencing studies have shown the ubiquity of genes coding for Hlips across diverse cyanobacterial taxa, ranging from marine to freshwater ecosystems. Notably, the abundance of the *hli* gene varies among species. For instance, the marine cyanobacterium *Prochlorococcus* MED4 harbors more than 20 *hli* genes, whereas the evolutionarily primitive, thylakoid-less species *Gloeobacter violaceus* contains five such genes (Bhaya *et al.*, 2002), in comparison to Synechocystis that has only four.

The genome of the model cyanobacterium *Synechocystis* PCC 6803 (hereafter *Synechocystis*) encodes four Hlips, nominally referred to as HliA, HliB, HliC and HliD (Fig. 6). Additionally, an Hlip domain, similar to HliC, is fused to the C-terminus of the ferrochelatase enzyme, a conserved feature in all types of oxygenic phototrophs (Sobotka *et al.*, 2011).

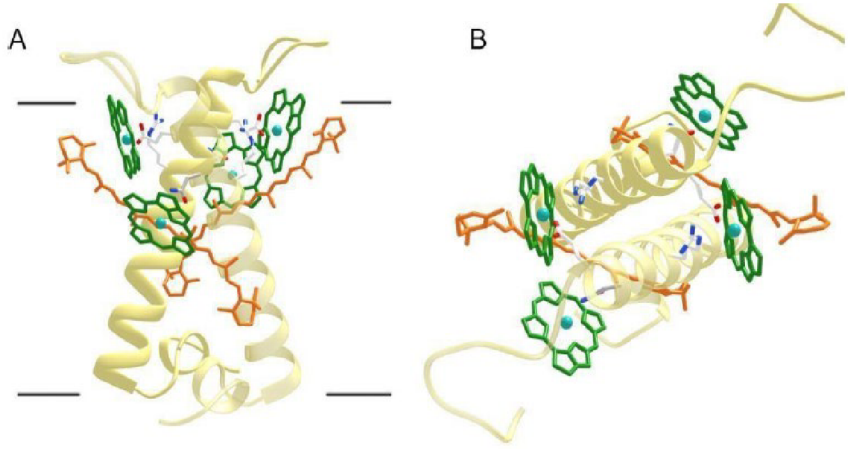

Fig. 5: Model of the Synechocystis HliC dimer. *View of HliC in the membrane (A) and view of the HliC dimer from the stroma (B). The HliC dimer binds two β-Cars molecules and four Chl-a molecules (Shukla et al., 2018).*

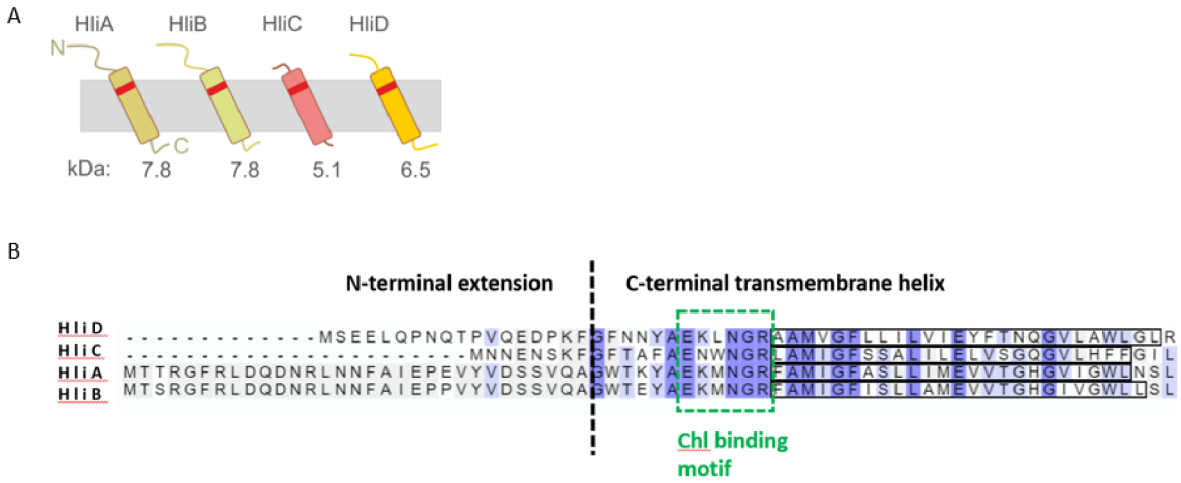

Fig. 6: A scheme of four Hlips encoded within the Synechocystis genome and the alignment of their amino acid sequences. *A) Proteins are designated as HliA-D. The gray ribbon represents the membrane. From the left, HliA and HliB are very similar, see (B); molecular masses of all four Hlips are also indicated. The conserved Chl-binding motif ExxNGR is highlighted by a red rectangle.* ***B)*** *Residues exhibiting absolute identity are marked in deep purple, while high-similarity residues are shown in light purple. Notably, the N-terminal extensions in HliA and HliB proteins are almost identical. The dashed line indicates less N-terminal extension, unique for HliA/B, HliC, and HliD, the C-terminal transmembrane helix is more conserved. The Chl-binding ExxNGR motif is shown by a green rectangle.*

Role of Hlips in PSII assembly

An efficient process of assembly of PSII is crucial for the proper functioning of photosynthetic machinery, particularly under stress conditions. Building of PSII in the cell occurs through a highly orchestrated series of events and involves the integration of multiple subunits and assembly factors. That includes integrating four so-called assembly modules, each containing one large, Chl-binding subunit (D1, D2, CP43, and CP47) (Komenda *et al.*, 2012b). These modules are already pre-loaded with Chl and Car cofactors before their incorporation into larger PSII assembly intermediates (Nixon *et al.*, 2010).

Assembly modules combine in a stepwise fashion (Fig. 7), starting with the dimerization of D1 and D2 modules to form the core of the PSII reaction center, commonly referred to as RCII. Next, the attachment of the CP47 module occurs, leading to an intermediate termed RC47 (Dobáková *et al.*, 2009; Boehm *et al.*, 2012). Further assembly steps involve the addition of the CP43 module, resulting in a monomeric (non-oxygen evolving) PSII core complex known as RCCII. The final step is the binding of lumenal subunits and the dimerization of the whole active PSII complex (Becker *et al.*, 2011).

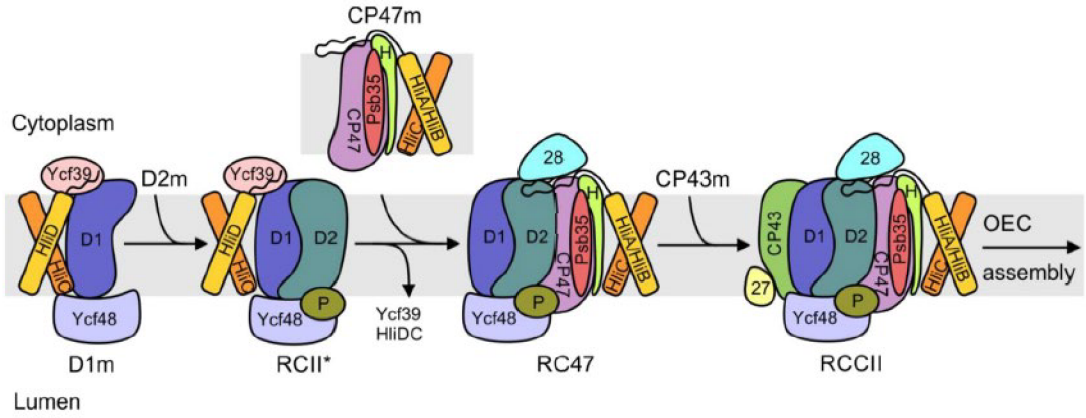

Fig. 7: A model showing the association of Hlips with different assembly intermediates of PSII in Synechocystis. *Starting from the left, the early assembly intermediates, namely D1 and D2 modules (D1m and D2m), combine to form the RCII complex. D1m binds the auxiliary proteins Ycf39 together with HliC/D heterodimer and the lumenal factor Ycf48. In the next step, the CP47 module (CP47m) integrates into the complex, leading to the complex named RC47. Under stress conditions, this complex contains Hlips attached to CP47 (either HliA/C or HliB/C pair). After this, the addition of CP43m and other components transitions the assembly to a more advanced stage, denoted as RCCII. As a later assembly step, the oxygen-evolving complex (OEC) incorporates, which results in an active monomeric PSII that can further dimerize (Koskela et al., 2020).*

The biogenesis of PSII is a dynamic process that involves continuous assembly, disassembly, and repair of the complex. PSII is also susceptible to photo-oxidative damage. Thus, the assembly factors and photoprotective proteins play crucial roles in maintaining the activity of PSII under various environmental conditions (Bricker *et al.*, 2015). Repair cycles likely share similarities with the assembly process regarding protein facilitators and intermediate complexes. Auxiliary proteins, which are parts of the mature PSII, participate in various stages of assembly and repair. For instance, proteins like Ycf48 and CyanoP are known to be associated with the RCII complex, whereas Psb28 and Psb27 are connected to the CP47 and CP43 modules and assembly intermediates in later stages. (Vass, 2012; Komenda *et al.*, 2012b; Järvi *et al.*, 2015).

In *Synechocystis*, the process of PSII assembly involves all four Hlips. The HliC and HliD proteins form a pigmented heterodimer, and this protein pair shows a strong binding affinity to the PSII assembly factor Ycf39 (Fig. 7). The resulting pigment-protein sub-complex, known as HliC/D-Ycf39, interacts with RCII, thereby generating a complex designated RCII* (Knoppová *et al.*, 2014). Ycf39 with Hlips dissociates from RCII before the RC47 intermediate is formed (Knoppová *et al.*, 2014). The exact role of the HliC/D-Ycf39 sub-complex is still not clear, but it might serve multifunctional roles. It can include quenching of excessive light energy via

energy transfer from Chl to β-Car and/or the protection of the newly formed PCII against photo-oxidative damage (Staleva *et al.*, 2015). Indeed, the HliC/D heterodimer has been shown to effectively dissipate excitation energy from the RCII complex (Knoppová, 2014). Moreover, it has been speculated that the HliC/D-Ycf39 facilitates the incorporation of Chl into the emerging D1 or D2 proteins because HliC/D Hlips also bind to the Chl synthase enzyme (Chidgey *et al.*, 2014).

In a broader context, homologs of HliC and HliD in plants, known as OHPs (one-helix proteins), also engage in similar interactions with their respective PSII components and a plant Ycf39 homolog, thereby indicating a conserved role of Hlips and OHPs in cyanobacteria and eukaryotic phototrophs (Myouga *et al.*, 2018; Hey and Grimm, 2018; Li *et al.*, 2019).

In contrast to HliD/C, the HliA/C and HliB/C heterodimers associate during stress with the CP47 module of PSII and remain attached to the assembling PSII during later stages (RCCII; Fig. 7. These heterodimers also bind Chl and β-Car in a quenched configuration, probably further contributing to the photoprotection mechanisms of PSII. (Koskela *et al.*, 2020). As noted above, Hlips can be associated with pigments only as dimers, and the HliC serves an important role as the second helix (Konert, 2022). Specifically, HliA and HliB most likely cannot form homodimers or mutual heterodimers (see later), and only in the absence of HliC, HliB can be co-isolated with a small amount HliD. HliA has been isolated exclusively as a heterodimer with HliC; in the *Synechocystis* Δ*hliC* mutant, the HliA proteins do not accumulate. This high specificity of HliA/B to HliC contrasts with the ability of HliC to interact with all other Hlips, including HliC itself (Staleva *et al.*, 2015; Shukla *et al.*, 2018). How certain combinations in Hlips pairing are structurally prevented remains enigmatic.

The recent study by Konert *et al.* (2022) further suggests that the extended N-terminal domains of HliA and HliB may hinder their dimerization capabilities, a process that is less constrained in HliC and HliD, presumably due to their shorter N-terminal regions. Moreover, the N-terminal sequences of HliA, HliB, and probably also HliD are expected to recognize and bind Hlip-interacting proteins involved in the PSII assembly. While the N-terminus of HliA and HliB probably binds the CP47 module in a similar way as described recently for the assembly factor Psb34 (Konert *et al.*, 2022), the N-terminal region of HliD could be sufficient for the binding of Ycf39 factor or Chl-synthase enzyme (Konert *et al.*, 2022).

OBJECTIVES OF THE WORK

Hlips are very small proteins. Still, they have the capacity to bind two different pigment cofactors in a well-tuned configuration, form a specific set of homo- and heterodimers (some combinations between Hlips are apparently forbidden), and, finally, recognize other protein partners (Ycf39 and Chl-synthase, CP47 module). Although there is accumulating knowledge about Hlips, including their essential roles in the photoprotection of PSII assembly, how Hlips recognize their protein partners is unclear.

This thesis aims to clarify the importance of the Hlip-specific N-terminus and the highly conserved transmembrane helix in preventing homo-dimerization of HliA and HliB and binding PSII-assembly-related protein. According to a recent hypothesis, the N-terminus is solely responsible for the recognizing of PSII factors and subunits, while the membrane helix somehow determines the specificity of Hlip-Hlip interactions. To address this model, *Synechocystis* strains producing chimeric Hlips have been synthesized, each fusing the N-terminal domain from one Hlip with the transmembrane helix from another. These proteins were purified, and the interaction with other proteins, as well as pigments, was characterized.

MATERIAL

Buffers for the isolation of His-tagged proteins

Thylakoid buffer: 25 mM MES/NaOH, pH 6.5, 20 mM $MgCl_2$, 20 mM $CaCl_2$
Equilibration buffer: (thylakoid buffer + 0.5 M NaCl + 10 mM Imidazole + 0.02 % β-Dodecyl-D-Maltoside (β-DDM) + 0.02% glycodiosgenin (GDN), 25% glycerol)
Wash buffer 1: 20 mM imidazole (in thylakoid buffer + 0.02 % β-DDM + 0.02% GDN, 25% glycerol)
Wash buffer 2: 40 mM imidazole (in thylakoid buffer + 0.02 % β-DDM + 0.02% GDN, 10% glycerol)
Elution buffer 1: 200 mM imidazole (in thylakoid buffer + 0.02 % β-DDM + 0.02% GDN, 10% glycerol)
Elution buffer 2: 400 mM imidazole (in thylakoid buffer + 0.02 % β-DDM + 0.02% GDN, 10% glycerol)

Buffers for clear-native gel

Gel buffer 6x: 3M aminocaproic acid, 300mM Bis-Tris/HCl, pH 7.6

Acrylamide solution: 50% AA, 0.83% BIS

Cathode buffer: 50 mM Tricine, 15 mM Bis-Tris/HCl, pH 7.0

Anode buffer: 50 mM Bis-Tris/HCl, pH 7.0

Buffers for denaturing acrylamide gel

Gel buffer: 2.8M Tris/HCl, pH 8.6

Acrylamide solution: 50% AA, 0.83% BIS

Cathode buffer: 25 mM Tris, 0.1.92 M glycine

Anode buffer: 25 mM Tris/HCl, pH 8.3

Kits for molecular biology used in the project

PureLink PCR Purification Kit (Thermo Scientific)

GeneJET Gel Extraction Kit (Thermo Scientific)

Fig. 7: Amino-acid sequences of chimeric Hlips*. The combination of N-terminal and C-terminal parts from HliA, HliC and HliD; HliA parts are depicted in red, HliC region are in grey and HliD in blue.*

METHODS

Construction of Synechocystis strains

At the beginning of the project, I prepared a set of *Synechocystis* mutants, each expressing chimeric *hli* genes under *psbA2* promoter (Fig. 7). Chimeric Hlips combining HliD with HliC were produced in Δ*hliD* mutant background:

his-hliAD

his-hliAC

his-hliDA

his-hliDC/ΔhliD

his-hliCA

his-hliCD/ΔhliD

To construct these strains, I amplified synthetic *hli* genes (purchased from GenScript) by Q5 PCR. After purification of the PCR product, genes were cloned into the pPD-FLAG-Km plasmid (Konert *et al.*, 2022) in a way that the C-terminal FLAG on the plasmid was eliminated, and 8xHis-tag was added at the N-terminus using primer sequence (see Table 1). Briefly, the PCR product and plasmid were digested with *Nde*I and *Bgl*II and ligated together using T4 ligase, and the ligation mixture was left at +4°C overnight. The next day, the restriction enzymes were partially inactivated for 20 min at +65°C. The mixture was then precipitated by adding 450 μl of butanol, vigorously vortexed, and centrifuged for 10 minutes at maximum speed at +4°C. The supernatant was discarded, and the pellet was washed with 400 μl 70% ethanol, dried in a flow hood, and resuspended in 10 μl H_2O.

Plasmids were electroporated into *E. coli* DH5α (1.8 kV), plated on LB-Amp100 antibiotic, and incubated at 37°C overnight. After purification of plasmids from *E. coli* utilizing the PureLink HiPure Plasmid Miniprep Kit (ThermoFisher), the cloning was verified by sequencing.

Table 1: List of primers used for the preparation of Synechocystis strains used in this study.

Strains	Primers
his-hliAD	HliA_fw_His8_*Nde*I + HliD-*Bgl*II
his-hliAC	HliA_fw_His8_*Nde*I + HliC-Strep*Bgl*II
his-hliDA	HliD_fw_His8_*Nde*I + HliA_rev_*Bgl*II
his-hliDC/ΔhliD	HliD_fw_His8_*Nde*I + HliC-Strep*Bgl*II
his-hliCA	HliC_fw_His8_*Nde*I + HliA_rev_*Bgl*II
his-hliCD/ΔhliD	HliC_fw_His8_*Nde*I + HliD-*Bgl*II

Primers	Sequences
HliA_fw_His8_*Nde*I	TAATAACATATGCACCATCACCATCACCATCACCATGGAACCACCCGTGGCTTC
HliC_fw_His8_*Nde*I	TAATAACATATGCACCATCACCATCACCATCACCATGGAAACAACGAAAACTCTAAATTT
HliD_fw_His8_*Nde*I	TAATAACATATGCACCATCACCATCACCATCACCATGGAAGTGAAGAACTACAACCG
HliA_rev_*Bgl*II	TAATAAAGATCTCTACAGGCTATTTAACCAAC
HliC-Strep*Bgl*II	AGGAACTATGAGATCTTTACAGAATGCCGAAGAAGT
HliD-*Bgl*II	GCTATGAGATCTAGCGCAGTCCCAACCAGG

Synechocystis transformation

Synechocystis WT-P (Tichý *et al.*, 2016) or Δ*hliD* (Chidgey *et al.*, 2014) cells suspension in BG11 were mixed with plasmid DNA and incubated in light for approx. 3 hours. The mixture was transferred on a plate without selection and left in a grow chamber overnight. The next day, cells were streaked to Km plates (10 mg l^{-1}) and grown under light for 1-2 weeks. After that, the colonies were restreaked several times on the plates with increasing concentrations of Km to segregate the mutated locus into all copies of the chromosome. Segregation was checked by PCR, and the fully-segregated colonies were replanted on a plate without antibiotics and, after one week of growth, were screened again for stability.

Growth conditions

To obtain ~4l of *Synechocystis* cells for protein purification, strains were first inoculated in 50 ml of BG11 in a 250 ml Erlenmeyer flask and grown for two days. The culture was then diluted to 100 ml (OD_{750} 0.12, Genesys spectrophotometer) with BG11 to 500 ml Erlenmeyer flask and let grow for one more day to OD_{750} ~0.70. The culture was then diluted into six 1l cylinders (500 ml of BG11 + 100 ml starting culture) and grown with air bubbling and stirring for ~3 days at 50 µmol photons m^2. To increase the expression of chimeric *hli* genes, the culture was treated with high light (500 µmol photons m^2) for 5 h and harvested at OD_{750} ~0.6 (not over 1.0). The harvested cells were transferred to 1l bottles (Sorvall Lynx) and centrifuged at

28,000 × g for 10 minutes at +4°C. The pellets were resuspended in thylakoid buffer and transferred to 5 ml falcons.

Isolation of TMs

A protease inhibitor (Roche Complete without EDTA) was added into cell suspension, and the cells were then broken on a bead beater with balotina beats (100-200 µm) using 8 cycles of 1-minute beating and 4 minutes of cooling on ice. The glass beads were washed off with thylakoid buffer. The broken cell suspension was then centrifuged at 53,000 × g for 20 minutes at 4°C, the supernatant discarded, and the pellet resuspended in thylakoid buffer, then centrifuged again with the same settings. Finally, the supernatant was discarded, and the pellet (thylakoid membranes) was resuspended in a small volume of thylakoid buffer. A small aliquot was taken for Chl concentration measurement in methanol as described in Lichtenthaler and Wellburn 1983, and the rest was frozen in liquid nitrogen and stored at - 80°C.

Protein purification

Thylakoid membranes were solubilized using 1% β-DDM at a ~0.5 $\mu g\ \mu l^{-1}$ Chl concentration. An EDTA-free protease inhibitor (Sigma-Aldrich) was added, and the mixture was incubated, avoiding light, with slow rotation at 10-12 RPM for 30 minutes at ~ 10°C. Then, 1% GDN was added and kept slowly rotating (to avoid excessive foam creation) for 10 more minutes. After solubilization, the mixture was centrifuged at 47,500 × g for 30 minutes at +4°C to pellet the insoluble material.

The Ni-NTA resin (Protino, Macherey-Nagel) was prepared into 10 ml chromatography columns (Poly-Prep, Bio-Rad). For every 5 mg of Chl, 200 µl of resin was used, washed with water, then washed with equilibration buffer (2 × 5 column volume). To solubilized TM were added 0.5 M NaCl and 10 mM imidazole (6.5 pH) final concentration and the mixture was transferred to the chromatography column with the pre-equilibrated Ni resin. The column was closed and kept on slow rotation for 1 h at 10°C in the dark.

After incubation, the resin was washed with 20 column volumes (CV) of equilibration buffer, 20 CV of washing buffer 1 (20 mM imidazole), and 20 CV of washing buffer 2 (40 mM Imidazole). The elution was performed by 10 CV of elution buffer 1 (200 mM imidazole). In the case of an eluate without any visible coloration, the elution buffer 2 (400 mM imidazole)

was used in an additional step. The final elutions, if colored, were combined and concentrated with a 50 kDa MW cut-off spin column (Millipore) to a final volume of ~150 µl.

Absorption spectra of eluted proteins

To acquire absorption spectra of pigments associated either with purified Hlips or with co-isolated proteins, spectra of elutions were determined immediately after Ni affinity chromatography. Spectra measurements were taken in the range of 350 nm - 750 nm using a Shimadzu UV-3000 spectrophotometer.

CN-PAGE

To prepare the 4-14% gradient native gel, three distinct acrylamide solutions were combined: 4% and 14% for the gradient resolving gel, and an additional 4% for the stacking gel. Before pouring, 38 and 19 µl of 10% freshly prepared ammonium persulfate (APS) were added to the 14% and 4% acrylamide mixtures, respectively. Following the formation of the 4-14% gradient, the gel surface was covered with distilled water and allowed to undergo polymerization for 1 h. Subsequently, the water was drained using a syringe, a comb was positioned to create wells, and the gel was layered with the 4% top gel. Prior to this step, 40 µl of APS was mixed with the solution for the stacking gel. A layer of distilled water was added to protect the gel surface, and the gel was allowed to set for an additional 1 hour and 30 minutes. The gel-containing slides were then fixed into the Bio-Rad Protean II xi cell apparatus. The upper chamber of the equipment, which housed the gels, was filled with cathode buffer, while the lower chamber was supplemented with anode buffer. Each sample was then incubated with 1% A8-35 amphipol, 1% DDM, and 1% GDN for 5 min on ice (Kameo *et al.*, 2021; Tribet *et al.*, 1996). After loading the samples, the apparatus was tempered to 4°C, and protein separation was run at 1000 V for 60 minutes.

SDS-PAGE and the second dimension after the CN-PAGE

To prepare the 16-20% gradient SDS gel, three different acrylamide solutions were combined: 16% and 20% for the resolving gradient gel and 5% for the stacking gel. 360 µl of 10% SDS and 36 µl of 10% APS were added to the 16% and 20% acrylamide mixtures before pouring. After mixing a 16-20% gradient, the gel was covered with distilled water and allowed to undergo polymerization for 1 hr. Subsequently, the water was removed using a syringe, and the

gel was overlaid with 5% stacking gel containing 180 μl of 10% SDS and 36 μl of 10% APS. The gel was then covered with distilled water and polymerized for 1.5 h. After removing distilled water, the gel-containing slides were fixed into the Bio-Rad Protean II xi cell apparatus. The upper chamber of the device was filled with cathode buffer, while the lower chamber was filled with anode buffer. A strip (approximately 1 cm wide) of clear-native gel was denatured in a solution containing 1% DDT and 1% SDS for 20 min, and this strip was then placed atop the denaturing gel. Protein separation ran at 16 mA, 350 V for 16 hours with the apparatus maintained at 23°C. For the subsequent analyses, gels were stained with Coomassie blue.

HPLC pigment analysis

To analyze pigments associated with His-tagged Hlips, a small segment of the CN gel containing Hlips was cut and further cut into small pieces. They were incubated overnight in 200 µl of 20 mM MES buffer pH 6.5 with 0.04% β-DDM to elute Hlips from the gel. Pigments extracted from Hlips by 75% methanol were injected into Agilent-1260 High-Performance Liquid Chromatography (HPLC) system with a diode-array detector. The separation runs on a Zorbax Eclipse C18 column, 3.9 × 250 mm and a particle size of 5 μm with 35% (v/v) methanol and 15% (v/v) acetonitrile in 0.25 M pyridine (solvent A) and 20% (v/v) methanol, 20% (v/v) acetone, 60% (v/v) acetonitrile as solvent B. Pigments were eluted with a linear gradient of solvent B (30–95% (v/v) in 35 min) in solvent A followed by 95% of solvent B in solvent A at a flow rate of 0.8 ml per minute at 40 °C. Chl-*a* and Cars were detected at an absorbance of 440 nm, and the integration of the peak areas ensued. The molar stoichiometry of the pigments was ascertained through the comparison with calibration curves derived from authentic standards.

RESULTS

In order to elucidate the role of the N-terminal domain and transmembrane helix in the mutual binding of Hlips as well as in recognizing of non-Hlip protein partners, I first prepared *Synechocystis* strains that are producing chimeric 8×His-tagged Hlips (see Fig. 7), specifically: *his-hliAC*, *his-hliCA*, *his-hliAD*, *his-hliDA*, *his-hliCD*/Δ*hliD*, and *his-hliDC*/Δ*hliD*. Strains were named as a combination of two domains; e.g., his-hliAC cells produce a new protein containing the N-terminal domain from HliA and the C-terminal domain from HliC. I did not make combinations with HliB as this protein is very similar to HliA (see Fig. 6), and the results obtained for HliA should be valid also for the HliB. As the HliD can form homodimers (HliD-HliD), the presence of HliDC-HliD and HliCD-HliD heterodimers would make it challenging to identify proteins (Ycf39 and ChlG) interacting physically with chimeric HliDC and HliCD and not via a native HliD copy. *His-hliCD* and *his-hliDC* constructs were, therefore, transformed into the Δ*hliD* genetic background.

For the isolation of Hlips, *Synechocystis* strains were initially grown under standard light conditions (40 μmol photons $m^{-2}s^{-1}$) until reaching an optical density at 750 nm (OD750) ~ 0.7. Following this, the cultures were scaled up (3l in total) and incubated for an additional three days until OD750 ranged between 0.6 and 1. To enhance the expression of *hli* genes that were placed under the high-light inducible *psbA2* promoter, light intensity was increased to 500 μmol $m^{-2}s^{-1}$ for 2-3 hours prior to cell collection. TM were extracted and then solubilized with a mixture of mild detergents (β-DDM and GDN) to preserve protein-protein interactions (Chae *et al.*, 2012). Proteins were subsequently purified on a nickel column as described in the Methods section.

Obtained eluates exhibited distinct colors: HliCA was dark yellow, HliCD was brown, HliAD was yellow-green, HliDA was yellow, HliDC was a darker brown, and HliAC was colorless. Absorbance spectra were measured immediately after purification, which also showed quite different concentrations (total yield) of Chl and carotenoids, although proteins were isolated from a similar volume of cells (Fig. 8). Spectra of HliDA, HliCA, HliCD, and HliDC appeared similar with relatively high content of carotenoids per Chl, but the HliAD eluate contained much less carotenoids per Chl. After measurement, eluates, approximately 4 ml each, were concentrated down to around 150 μl using 50 kDa molecular weight cut-off spin columns (Millipore).

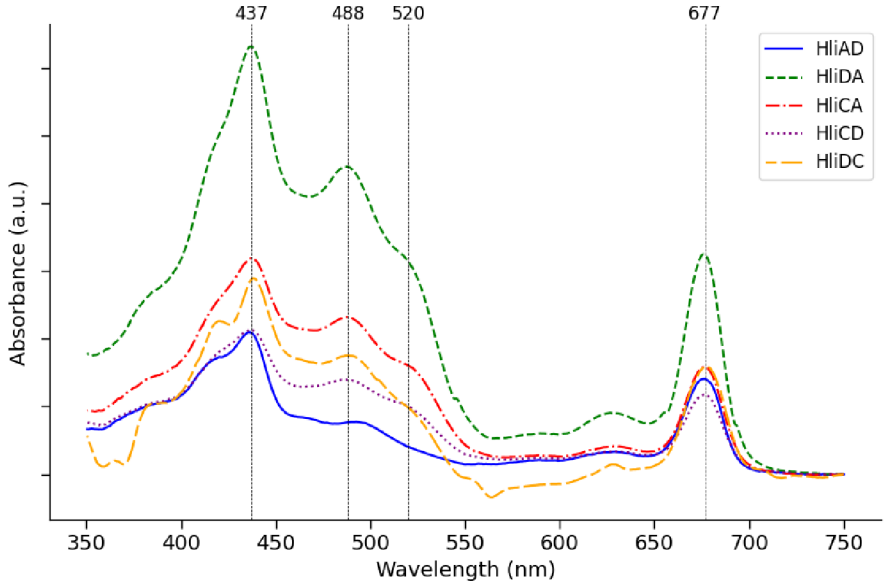

Fig 8: Absorbance spectra of the protein eluates from the nickel affinity chromatography. *Absorbance spectra of indicated elutions were recorded in the wavelength range of 350 nm to 750 nm. Vertical lines highlight the absorption maxima of Chl-a (437 nm and 677 nm) and Cars (488 nm and 520 nm). The HliAC eluate contained negligible pigment content and was not measured.*

Clear-native electrophoresis (CN-PAGE) was employed to identify proteins co-eluted with chimeric Hlips and to analyze pigments associated with these proteins. Approximately one-third of each concentrated eluate was mixed with 1% A8-35 amphipol and 1% GDN. In order to determine whether there are pigment-protein complexes able to dissipate energy, the CN-PAGE gel was first scanned for Chl fluorescence (Chl FL) under blue light illumination using a Fuji LAS 4000 system. A small piece of the non-fluorescent, yellow-orange band, typical for Hlips (Konert *et al.*, 2022), was cut from the gel for the later pigment analysis. The strip of CN-gel was then separated in the second dimension by SDS-PAGE and stained by Coomassie blue. This analysis was uniformly applied to all eluates.

Fig. 9 shows the 2D-gel analysis of HliAC and HliCA eluates. The HliAC protein contains the N-terminus from HliA, and as discussed later, this segment could be sufficient for the binding to the CP47 assembly module even in the case the transmembrane helix is from HliC. Unfortunately, for this variant, the only eluted proteins are monomeric and trimeric PSI, which are well-known contaminants of our nickel-affinity chromatography (see Konert *et al.* 2022). On the stained 2D SDS-gel, there are no visible Hlips, which suggests that HliAC does not

accumulate in the cell. This preparation can, therefore, also serve as a control 'WT' pulldown for this study.

Conversely, the HliCA protein, containing a very short N-terminal part from HliC and the transmembrane helix from HliA, was expected not to show any interaction with PSII subunits (CP47). Indeed, PSII was co-eluted with this chimeric Hlips. CN-PAGE, however, revealed a prominent pigmented band with no Chl fluorescence that apparently co-migrated with a hetero-dimer of Hlips observed on the stained SDS-PAGE. As verified by protein mass-spectrometry (data not shown), the lower-mass Hlip is HliC (Fig. 9). Despite the ability of the native HliC to form heterodimers with HliA/B or HliD, these proteins are not visible on the stained gel.

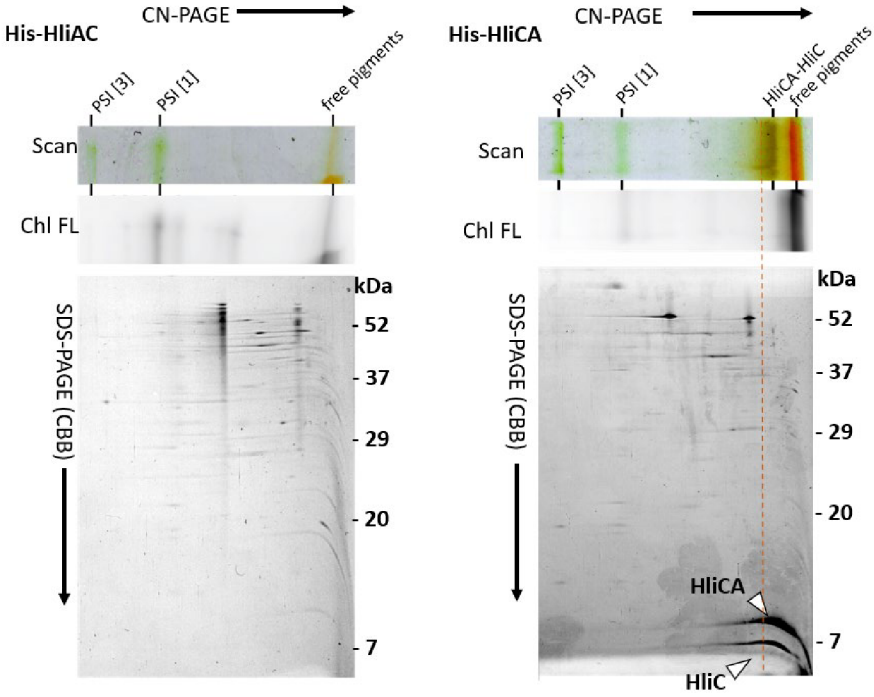

Fig. 9: 2D CN/SDS-PAGE separation of HliAC and HliCA pulldowns*. Proteins were isolated in a thylakoid buffer after solubilization by a mixture of β-DDM and GDN. The obtained CN-PAGE gel strip was scanned for Chl fluorescence after blue light illumination (Ch FL) using Fuji LAS 4000 before denaturation. The protein complexes were then separated by SDS electrophoresis (SDS-PAGE), and the resulting gel was stained with Coomassie blue (CBB). Analysis of HliAC and HliCA is left and right, respectively.*

The native HliD typically forms a dimer with HliC and the resulting HliD/C pair associates either with Ycf39 (and consequently with RSII) or with Chl synthase (ChlG). However, if the HliC is not expressed under low stress conditions, HliD-HliD homodimers accumulate in the cell, still binding Ycf39 or ChlG (Wysocka A, unpublished data). The interaction between HliD and HliA/B appears to be very weak and can be detected only in the Δ*hliC* mutant (Koskela *et*

al., 2022). According to our model, the HliDC protein, with the transmembrane helix from HliC, should be able to pair with all other Hlip. However, if the N-terminal domain of HliD plays a structural role in recognizing other Hlips, this chimeric protein might not bind to HliA/B. The CN-PAGE indicated the presence of RCCII (with corresponding subunits shown on 2D SDS PAGE, i.e., CP47, CP43, D2, and D1), RC47 and free CP47, and CP43 modules. Notably, the Chl FL profile revealed energy quenching in the CP47-Hlips complex (Fig. 10). Using mass spectrometry, we also identified a spot of the Ycf39 assembly factor (data not shown) but not Ch synthase. HliDC was apparently copurified with HliC but also with HliB or HliA, as confirmed by mass spectrometry.

HliCD protein, containing the transmembrane helix from the native HliD, showed potential pairing with HliC. No other specific interactors were detected. As the protein is very small, it comigrated with detergent micelles and free pigments (Fig. 10), which precluded pigment analysis.

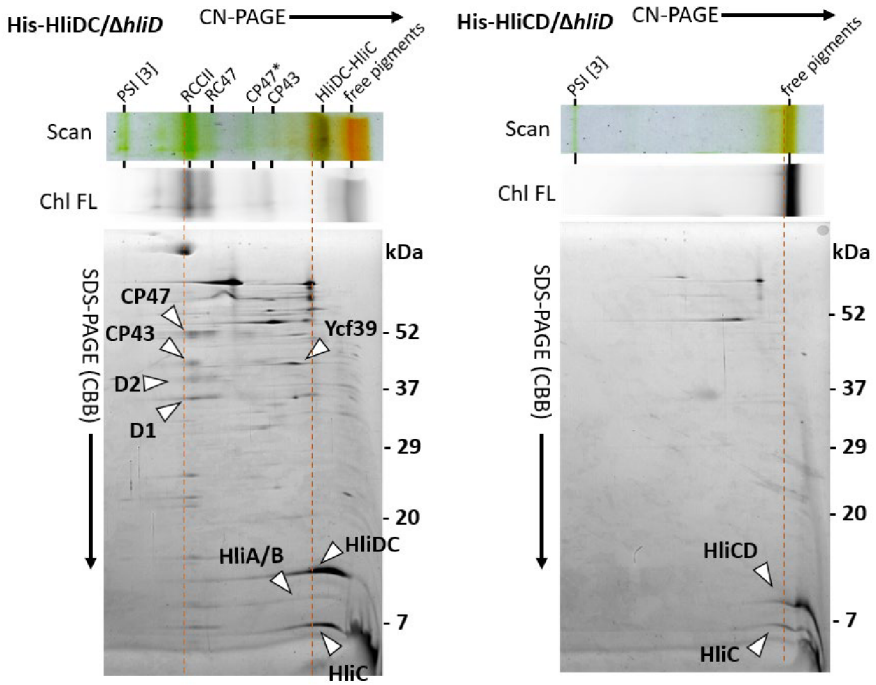

Fig. 10: 2D CN/SDS-PAGE separation of HliDC and HliCD protein complexes*. Both chimeric proteins were isolated in thylakoid buffer after solubilization in β-DDM and GDN. The obtained CN-PAGE gel strip was scanned for Chl fluorescence after blue light illumination (Ch FL) using Fuji LAS 4000 before denaturation. The protein complexes were then separated by SDS electrophoresis (SDS-PAGE), and the resulting gel was stained in Coomassie blue (CBB). CP47* indicates a 'free'CP47 module associated with Hlips. Left HliDC. Right: HliCD.*

Fig. 11 shows the analysis of purified HliAD. Similarly to HliDC, PSII assembly intermediates (RCCII, RC47, and CP47 module) have also been co-isolated with this Hlip. The Chl FL signal demonstrates the energy dissipation in CP47 associated with Hlips, which is a sharp difference when compared to highly-fluorescent CP47 only. The SDS-PAGE separated the individual components of these subunits, confirming the presence of HliAD and HliC, as well as PSII core subunits. However, no evidence of potential Ycf39 subunit association, as expected beforehand, was shown. In contrast to HliAD, the HliDA co-purified only with HliC and, apart from the pigmented HliDA-HliC dimer, another colored band with a slightly higher mass is visible on the gel and corresponds most likely to a tetrameric Hlip complex. The Chl fluorescence profile demonstrates a quenching conformation of pigments associated with Hlips.

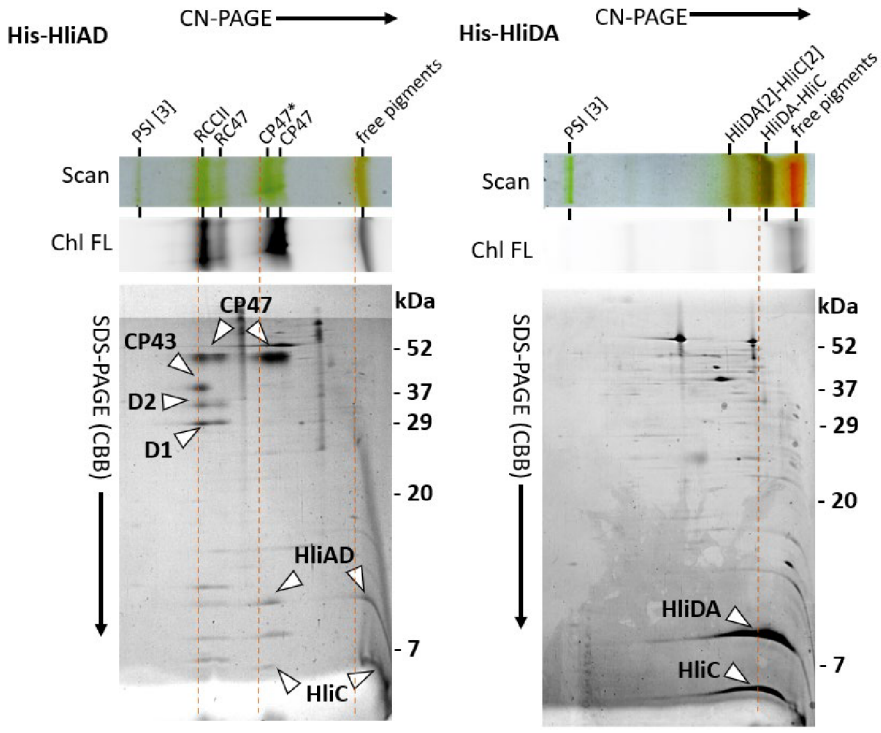

Fig. 11: 2D CN/SDS-PAGE separation of His-HliAD and His-HliDA protein complexes*. Both proteins were isolated in thylakoid buffer after solubilization by a mixture of β-DDM and GDN. The obtained CN-PAGE gel strip was scanned for Chl fluorescence after blue light illumination (Ch FL) using Fuji LAS 4000 before denaturation. The protein complexes were then separated by SDS electrophoresis (SDS-PAGE), and the resulting gel was stained in Coomassie blue (CBB). CP47* indicates a 'free' CP47 module associated with Hlips. Left His-HliAD. Right: His-HliDA.*

To identify pigments specifically associated with purified Hlips, I used HPLC analysis (Figure 12). A 3 × 2 mm section of the CN gel containing the Hlip complex was cut into small pieces and incubated overnight with 0.04% β-DDM in thylakoid buffer. After centrifugation,

the supernatant (~50 µL) was extracted and mixed with 150 µL of methanol injected into the HPLC machine.

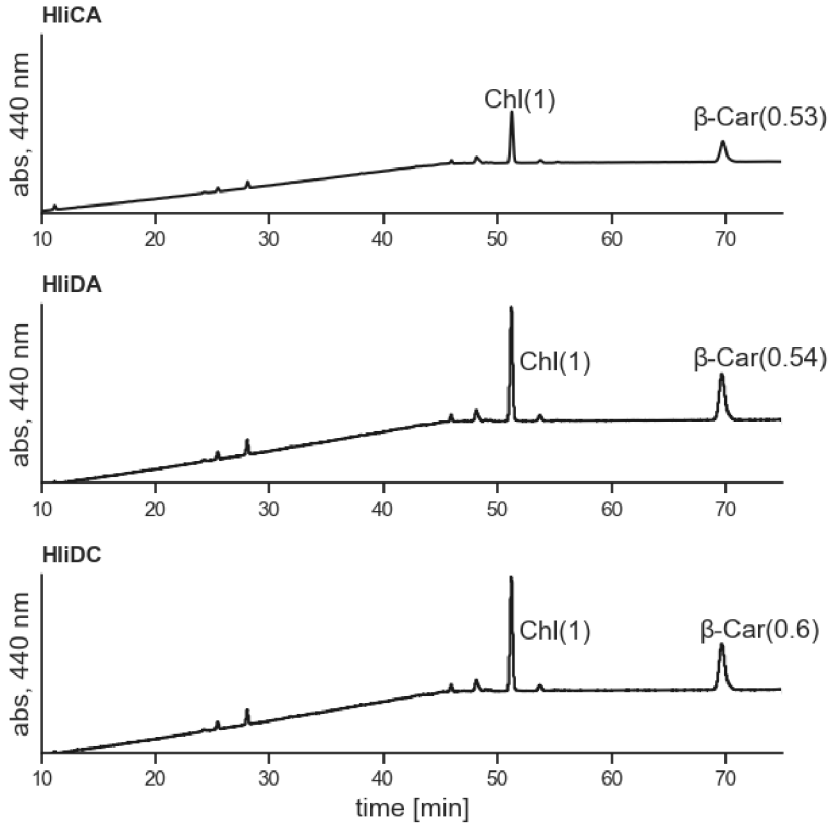

Fig. 12: HPLC analysis of pigments associated with Hlips. *Small sections of the CN gel containing the purified Hlips were carefully cut out and immersed in MES buffer (pH 6.5) containing 0.04% β-DDM. Pigments were extracted using 75% methanol and subjected to HPLC analysis. The chromatograms depicted in the figure correspond to the pigments extracted from HliCA, HliDA, and HliDC. Abs, 440 nm = absorbance measured at a wavelength of 440 nm, time = the retention time of the pigments from the column. Values in parentheses indicate the molar stoichiometry of Chl and β-Car.*

For the HPLC analysis, only 3 Hlips samples with sufficient concentration of pigments in the CN-gel were selected. The results in Fig. 12 revealed that all analyzed Hlips bind Chl-*a* and β-Car. For the HliCA and HliDA protein, the calculated Chl to β-Car ratio was approximately 1:0.5. For HliDC, this ratio was only slightly different at 1:0.6, indicating a probable pigment ratio of Chl : β-Car 5:3. The level of other carotenoids was very low.

DISCUSSION

In this work, I aimed to elucidate the structural basis of the interaction between Hlips themselves and with partner proteins in the model cyanobacterium *Synechocystis*. I characterized six chimeric Hlips, each containing an N-terminal domain from one Hlip combined with a transmembrane helix from another (Fig. 7). The findings reveal some interesting insights into the structural organization and functional dynamics of Hlips in cyanobacterial photosynthesis and stress responses.

Consistent with Konert *et al*. (2022), my results support the model that the hetero-dimerization of Hlips is essential not just for the binding of pigments but also with other proteins, such as PSII subunits. HliC and HliD are capable of forming homodimers, but HliA and HliB strictly form heterodimers with HliC (see Fig. 13). Although in the absence of HliC, the HliD is found as a homodimer (Wysocka A., unpublished data), levels of HliA and HliB are very low (Konert *et al*., 2022). It shows a crucial role for HliC in the stability and localization of these proteins.

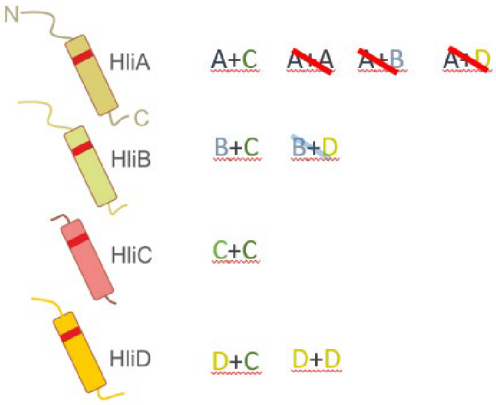

Fig. 13: The capability of individual Synechocystis Hlips to form homo- and heterodimers. *The illustration presents four Hlips: HliA, HliB, HliC, and HliD. Both HliA and HliB almost exclusively dimerize with HliC while avoiding dimerization with each other. HliC displays versatility, forming dimers with all, including itself. In contrast, HliD is able to homodimerize, but the functional unit is probably a heterodimer with HliC. In the absence of HliC, a small amount of HliB-HliD dimer can be observed, but not the HliA-HliD complex (Konert et al., 2022).*

The heterodimers formed by HliAD and HliCD with HliC, demonstrate that the transmembrane helix of HliD is sufficient to form a tight pigmented dimer with HliC. It is notable that although the HliAD protein is produced in the WT background and the native HliD should be present, I

did not co-purify a significant level of HliD. The situation with HliD might be, therefore, more complicated, and the formation of HliD homodimer is stabilized by a conserved motif located in the N-terminus (see Fig. 14).

Chl FL analysis revealed that the HliAD-HliC heterodimer associates with CP47 in a quenching formation, facilitating energy dissipation from all Chl in the complex. This is remarkable because CP47 contains 16 Chl and all absorbed energy needs to flow into the attached Hlip. Since the CP47 module is known to bind HliA/B (see Fig. 15), this again supports the model that the N-terminal region of HliA/B alone facilitates the attachment to the CP47 module, as proposed by Konert (2022). The HliD is known to bind the Ycf39 factor (Fig. 15) and Chl-synthase. However, such stable interactions were not observed for the HliAD protein. The N-terminal region from HliA is completely different from the HliD (see Fig. 14), probably hinders the ability of HliAD to bind Ycf39. On the other hand, the N-terminal region from HliC consists of only a few amino acids and probably does not bind any other protein. Indeed, the HliCA did not bind any known Hlip interactor.

The analysis of HliDC provides evidence that the binding of Ycf39 by HliD does not require the HliD transmembrane segment; the HliD N-terminus is apparently sufficient, which is in line with the predicted AlphaFold model (Fig. 15). On the other hand, a significant level Ch-synthase was not purified with any of the HliD-containing chimeric Hlips (HliDA, HliAD, HliDC, HliCD). The Chl-synthase-Hlips complex requires xantophylls for stability (Proctor *et al.*, 2020) and, indeed, such a complicated pigment-protein assembly might rely on specific residues from both N-terminal and transmembrane segments of HliD.

Co-purification of HliA/B (attached to RCCII) with HliDC highlights the ability and universality of the HliC transmembrane helix to bind tightly other Hlips since the HliD does not form dimers with HliA/B (Fig. 13). The motif preventing the HliD to interact with HliA/B is thus most likely inbuilt in the helix, not in the N-terminal domain. Interestingly, HliD-type Hlips contain highly-conserved arginine residue in the ERxNGR motif (Fig. 14), and it might be speculated that this residue modules the interaction with other Hlips and perhaps even with Chl-synthase. HliAC did not accumulate in the cell, suggesting that certain chimeric constructs are unstable.

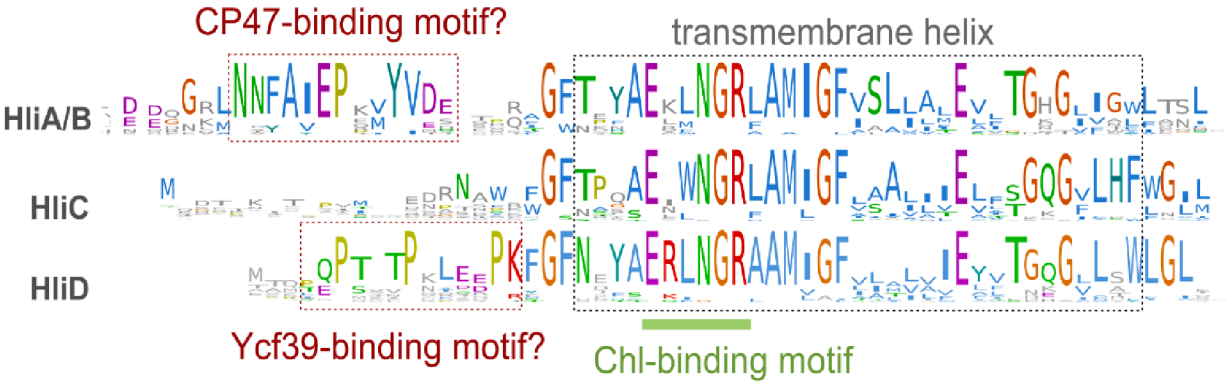

Fig. 14: Sequence web logo for HliA/B, HliC, and HliD types of Hlips*. The hli gene sequences were obtained from all available cyanobacterial genomes. Highlighted are possible motifs for the binding of CP47, Ycf39, and Chl pigments (Courtesy of Jan Janouškovec, unpublished).*

The Chl to β-Car ratios, measured by HPLC analysis for HliCA and HliDA, was approximately 1:0.5, close to the ratio reported by Shukla et al. (2018), corresponding to 4 Chls and 2 Cars. In contrast, HliDC showed a slightly different ratio, 1:0.6, suggesting a unique pigment binding configuration, with a probable pigment ratio of Chl: β-Car 5:3. This is the ratio reported by Koskela *et al*. (2022) for HliC-HliA/B heterodimers with a hypothetical third weaker Car binding site. My results show that the ability to bind Chl and Cars is robust and probably embedded in the transmembrane helix itself across different Hlips. The N-terminal region seems to play no role in pigment binding.

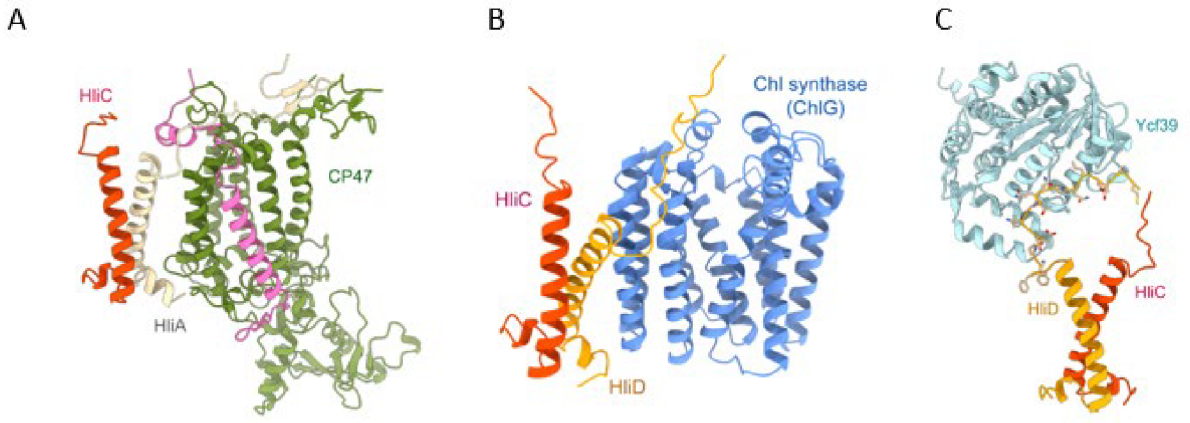

Fig. 15: Predicted interactions between Hlips and their partner proteins calculated using Alphafold2 multimer. *A) heterodimer composed of HliC and HliA is depicted in a complex with the CP47 assembly module. The PsbH subunit is shown in magenta. B) HliC-HliD heterodimer associated with Chl synthase. C) The predicted structure of the HliC-HliD-Ycf39 complex; according to this model, only the HliD N-terminus binds Ycf39 (Sobotka R., unpublished).*

In future work, to further validate these findings, I propose incorporating immunodetection of ChlG, Ycf39, HliA/B, and HliD using antibodies. Mass spectrometry of the complete elutions is also recommended. Additionally, exploring the necessity of the HliD N-terminus for the HliD/D dimer in a WT background could provide further insights. A detailed structural analysis of these interactions and complexes would also offer a more comprehensive understanding of their functional roles and mechanisms.

In conclusion, this work adds to the growing body of knowledge on the functional diversity and significance of Hlips in cyanobacteria. By exploring the behavior of chimeric Hlips, I provided insights into their structural organization, interactions with PSII subunits, and roles in energy dissipation and PSII assembly. These findings pave the way for further exploration into the intricate mechanisms of Hlip-mediated photoprotection and structural features.

REFERENCES

Balsera, M., Uberegui, E., Susanti, D., Schmitz, R. A., Mukhopadhyay, B., Schürmann, P., & Buchanan, B. B. (2013). Ferredoxin: thioredoxin reductase (FTR) links the regulation of oxygenic photosynthesis to deeply rooted bacteria. *Planta*, *237*(2), 619–635. https://doi.org/10.1007/s00425-012-1803-y

Barber, J. (2012). Photosystem II: The Water-Splitting Enzyme of Photosynthesis. *Cold Spring Harbor Symposia on Quantitative Biology*, *77*(0), 295–307. https://doi.org/10.1101/sqb.2012.77.014472

Benson, A. A. (2002). Following the path of carbon in photosynthesis: a personal story. *Photosynthesis Research*, *73*(1/3), 29–49. https://doi.org/10.1023/A:1020427619771

Blankenship, R. E. (2008). *Molecular Mechanisms of Photosynthesis*. Wiley-Blackwell.

Bricker, T. M., Mummadisetti, M. P., & Frankel, L. K. (2015). Recent advances in the use of mass spectrometry to examine structure/function relationships in photosystem II. *Journal of Photochemistry and Photobiology B: Biology*, *152*, 227–246. https://doi.org/10.1016/j.jphotobiol.2015.08.031

Chae, P. S., Rasmussen, S. G. F., Rana, R. R., Gotfryd, K., Kruse, A. C., Manglik, A., Cho, K. H., Nurva, S., Gether, U., Guan, L., Loland, C. J., Byrne, B., Kobilka, B. K., & Gellman, S. H. (2012). A New Class of Amphiphiles Bearing Rigid Hydrophobic Groups for Solubilization and Stabilization of Membrane Proteins. *Chemistry – A European Journal*, *18*(31), 9485–9490. https://doi.org/10.1002/chem.201200069

Chidgey, J. W., Linhartová, M., Komenda, J., Jackson, P. J., Dickman, M. J., Canniffe, D. P., Koník, P., Pilný, J., Hunter, C. N., & Sobotka, R. (2014). A Cyanobacterial Chlorophyll Synthase-HliD Complex Associates with the Ycf39 Protein and the YidC/Alb3 Insertase. *The Plant Cell*, *26*(3), 1267–1279. https://doi.org/10.1105/tpc.114.124495

Dang, K.-V., Plet, J., Tolleter, D., Jokel, M., Cuiné, S., Carrier, P., Auroy, P., Richaud, P., Johnson, X., Alric, J., Allahverdiyeva, Y., & Peltier, G. (2014). Combined Increases in Mitochondrial Cooperation and Oxygen Photoreduction Compensate for Deficiency in Cyclic

Electron Flow in *Chlamydomonas reinhardtii*. *The Plant Cell*, *26*(7), 3036–3050. https://doi.org/10.1105/tpc.114.126375

Dolganov, N. A., Bhaya, D., & Grossman, A. R. (1995). Cyanobacterial protein with similarity to the chlorophyll a/b binding proteins of higher plants: evolution and regulation. *Proceedings of the National Academy of Sciences*, *92*(2), 636–640. https://doi.org/10.1073/pnas.92.2.636

Engelken, J., Brinkmann, H., & Adamska, I. (2010). Taxonomic distribution and origins of the extended LHC (light-harvesting complex) antenna protein superfamily. *BMC Evolutionary Biology*, *10*(1), 233. https://doi.org/10.1186/1471-2148-10-233

Falkowski, P. G., & Raven, J. A. (2007). *Aquatic photosynthesis* (2nd ed). Princeton University Press.

Field, C. B., Behrenfeld, M. J., Randerson, J. T., & Falkowski, P. (1998). Primary Production of the Biosphere: Integrating Terrestrial and Oceanic Components. *Science*, *281*(5374), 237–240. https://doi.org/10.1126/science.281.5374.237

Green, B. R., & Parson, W. W. (2003). *Light-Harvesting Antennas in Photosynthesis*. Kluwer Academic Publishers.

Havaux, M., Guedeney, G., Hagemann, M., Yeremenko, N., Matthijs, H. C. P., & Jeanjean, R. (2005). The chlorophyll-binding protein IsiA is inducible by high light and protects the cyanobacterium *Synechocystis* PCC6803 from photooxidative stress. *FEBS Letters*, *579*(11), 2289–2293. https://doi.org/10.1016/j.febslet.2005.03.021

He, Q., Dolganov, N., Björkman, O., & Grossman, A. R. (2001). The High Light-inducible Polypeptides in Synechocystis PCC6803. *Journal of Biological Chemistry*, *276*(1), 306–314. https://doi.org/10.1074/jbc.M008686200

Jordan, P., Fromme, P., Witt, H. T., Klukas, O., Saenger, W., & Krauß, N. (2001). Three-dimensional structure of cyanobacterial photosystem I at 2.5 Å resolution. *Nature*, *411*(6840), 909–917. https://doi.org/10.1038/35082000

Kameo, S., Aso, M., Furukawa, R., Matsumae, R., Yokono, M., Fujita, T., Tanaka, A., Tanaka, R., & Takabayashi, A. (2021). Substitution of Deoxycholate with the Amphiphilic Polymer Amphipol A8-35 Improves the Stability of Large Protein Complexes during Native

Electrophoresis. *Plant and Cell Physiology*, *62*(2), 348–355. https://doi.org/10.1093/pcp/pcaa165

Keeling, P. J. (2010). The endosymbiotic origin, diversification and fate of plastids. *Philosophical Transactions of the Royal Society B: Biological Sciences*, *365*(1541), 729–748. https://doi.org/10.1098/rstb.2009.0103

Komenda, J., Knoppová, J., Kopečná, J., Sobotka, R., Halada, P., Yu, J., Nickelsen, J., Boehm, M., & Nixon, P. J. (2012). The Psb27 Assembly Factor Binds to the CP43 Complex of Photosystem II in the Cyanobacterium *Synechocystis* sp. PCC 6803. *Plant Physiology*, *158*(1), 476–486. https://doi.org/10.1104/pp.111.184184

Komenda, J., & Sobotka, R. (2016). Cyanobacterial high-light-inducible proteins — Protectors of chlorophyll–protein synthesis and assembly. *Biochimica et Biophysica Acta (BBA) - Bioenergetics*, *1857*(3), 288–295. https://doi.org/10.1016/j.bbabio.2015.08.011

Komenda, J., & Sobotka, R. (2019). Chlorophyll-binding subunits of photosystem I and II: Biosynthesis, chlorophyll incorporation and assembly. In *Advances in Botanical Research* (Vol. 91, pp. 195–223). Elsevier. https://doi.org/10.1016/bs.abr.2019.02.001

Konert, M. M., Wysocka, A., Koník, P., & Sobotka, R. (2023). Correction: High-light-inducible proteins HliA and HliB: pigment binding and protein–protein interactions. *Photosynthesis Research*, *157*(1), 53–53. https://doi.org/10.1007/s11120-023-01016-y

Kopp, R. E., Kirschvink, J. L., Hilburn, I. A., & Nash, C. Z. (2005). The Paleoproterozoic snowball Earth: A climate disaster triggered by the evolution of oxygenic photosynthesis. *Proceedings of the National Academy of Sciences*, *102*(32), 11131–11136. https://doi.org/10.1073/pnas.0504878102

Koskela, M. M., Brünje, A., Ivanauskaite, A., Lopez, L. S., Schneider, D., DeTar, R. A., Kunz, H.-H., Finkemeier, I., & Mulo, P. (2020). Comparative analysis of thylakoid protein complexes in state transition mutants nsi and stn7: focus on PSI and LHCII. *Photosynthesis Research*, *145*(1), 15–30. https://doi.org/10.1007/s11120-020-00711-4

Kumar, K., Mella-Herrera, R. A., & Golden, J. W. (2010). Cyanobacterial Heterocysts. *Cold Spring Harbor Perspectives in Biology*, *2*(4), a000315–a000315. https://doi.org/10.1101/cshperspect.a000315

Liberton, M., Austin, J. R., Berg, R. H., & Pakrasi, H. B. (2011). Unique Thylakoid Membrane Architecture of a Unicellular N2-Fixing Cyanobacterium Revealed by Electron Tomography. *Plant Physiology*, *155*(4), 1656–1666. https://doi.org/10.1104/pp.110.165332

Lichtenthaler, H. K., & Wellburn, A. R. (1983). Determinations of total carotenoids and chlorophylls *a* and *b* of leaf extracts in different solvents. *Biochemical Society Transactions*, *11*(5), 591–592. https://doi.org/10.1042/bst0110591

Liu, L.-N. (2016). Distribution and dynamics of electron transport complexes in cyanobacterial thylakoid membranes. *Biochimica et Biophysica Acta (BBA) - Bioenergetics*, *1857*(3), 256–265. https://doi.org/10.1016/j.bbabio.2015.11.010

Liu, L.-N., Chen, X.-L., Zhang, Y.-Z., & Zhou, B.-C. (2005). Characterization, structure and function of linker polypeptides in phycobilisomes of cyanobacteria and red algae: An overview. *Biochimica et Biophysica Acta (BBA) - Bioenergetics*, *1708*(2), 133–142. https://doi.org/10.1016/j.bbabio.2005.04.001

Liu, Z., Yan, H., Wang, K., Kuang, T., Zhang, J., Gui, L., An, X., & Chang, W. (2004). Crystal structure of spinach major light-harvesting complex at 2.72 Å resolution. *Nature*, *428*(6980), 287–292. https://doi.org/10.1038/nature02373

Loll, B., Kern, J., Saenger, W., Zouni, A., & Biesiadka, J. (2005). Towards complete cofactor arrangement in the 3.0 Å resolution structure of photosystem II. *Nature*, *438*(7070), 1040–1044. https://doi.org/10.1038/nature04224

Mitchell, P. (1961). Coupling of Phosphorylation to Electron and Hydrogen Transfer by a Chemi-Osmotic type of Mechanism. *Nature*, *191*(4784), 144–148. https://doi.org/10.1038/191144a0

Müller, P., Li, X.-P., & Niyogi, K. K. (2001). Non-Photochemical Quenching. A Response to Excess Light Energy. *Plant Physiology*, *125*(4), 1558–1566. https://doi.org/10.1104/pp.125.4.1558

Nelson, N., & Ben-Shem, A. (2004). The complex architecture of oxygenic photosynthesis. *Nature Reviews Molecular Cell Biology*, *5*(12), 971–982. https://doi.org/10.1038/nrm1525

Nelson, N., & Yocum, C. F. (2006). STRUCTURE AND FUNCTION OF PHOTOSYSTEMS I AND II. *Annual Review of Plant Biology*, *57*(1), 521–565. https://doi.org/10.1146/annurev.arplant.57.032905.105350

Niedzwiedzki, D. M., Tronina, T., Liu, H., Staleva, H., Komenda, J., Sobotka, R., Blankenship, R. E., & Polívka, T. (2016). Carotenoid-induced non-photochemical quenching in the cyanobacterial chlorophyll synthase–HliC/D complex. *Biochimica et Biophysica Acta (BBA) - Bioenergetics*, *1857*(9), 1430–1439. https://doi.org/10.1016/j.bbabio.2016.04.280

Nixon, P. J., Michoux, F., Yu, J., Boehm, M., & Komenda, J. (2010). Recent advances in understanding the assembly and repair of photosystem II. *Annals of Botany*, *106*(1), 1–16. https://doi.org/10.1093/aob/mcq059

Pascual-Aznar, G., Konert, G., Bečková, M., Kotabová, E., Gardian, Z., Knoppová, J., Bučinská, L., Kaňa, R., Sobotka, R., & Komenda, J. (2021). Psb35 Protein Stabilizes the CP47 Assembly Module and Associated High-Light Inducible Proteins during the Biogenesis of Photosystem II in the Cyanobacterium *Synechocystis* sp. PCC6803. *Plant and Cell Physiology*, *62*(1), 178–190. https://doi.org/10.1093/pcp/pcaa148

Pazderník, M., Mareš, J., Pilný, J., & Sobotka, R. (2019). The antenna-like domain of the cyanobacterial ferrochelatase can bind chlorophyll and carotenoids in an energy-dissipative configuration. *Journal of Biological Chemistry*, *294*(29), 11131–11143. https://doi.org/10.1074/jbc.RA119.008434

Proctor, M. S., Pazderník, M., Jackson, P. J., Pilný, J., Martin, E. C., Dickman, M. J., Canniffe, D. P., Johnson, M. P., Hunter, C. N., Sobotka, R., & Hitchcock, A. (2020). Xanthophyll carotenoids stabilize the association of cyanobacterial chlorophyll synthase with the LHC-like protein HliD. *Biochemical Journal*, *477*(20), 4021–4036. https://doi.org/10.1042/BCJ20200561

Promnares, K., Komenda, J., Bumba, L., Nebesarova, J., Vacha, F., & Tichy, M. (2006). Cyanobacterial Small Chlorophyll-binding Protein ScpD (HliB) Is Located on the Periphery of

Photosystem II in the Vicinity of PsbH and CP47 Subunits. *Journal of Biological Chemistry*, *281*(43), 32705–32713. https://doi.org/10.1074/jbc.M606360200

Raines, C. A. (2003). The Calvin cycle revisited. *Photosynthesis Research*, *75*(1), 1–10. https://doi.org/10.1023/A:1022421515027

Raven, J. A., Beardall, J., Larkum, A. W. D., & Sánchez-Baracaldo, P. (2013). Interactions of photosynthesis with genome size and function. *Philosophical Transactions of the Royal Society B: Biological Sciences*, *368*(1622), 20120264. https://doi.org/10.1098/rstb.2012.0264

Sánchez-Baracaldo, P., & Cardona, T. (2020). On the origin of oxygenic photosynthesis and Cyanobacteria. *New Phytologist*, *225*(4), 1440–1446. https://doi.org/10.1111/nph.16249

Schlesinger, W. H., & Bernhardt, E. S. (2013). *Biogeochemistry: an analysis of global change* (Third edition). Elsevier/Academic Press.

Sessions, A. L., Doughty, D. M., Welander, P. V., Summons, R. E., & Newman, D. K. (2009). The Continuing Puzzle of the Great Oxidation Event. *Current Biology*, *19*(14), R567–R574. https://doi.org/10.1016/j.cub.2009.05.054

Shukla, M. K., Llansola-Portoles, M. J., Tichý, M., Pascal, A. A., Robert, B., & Sobotka, R. (2018). Binding of pigments to the cyanobacterial high-light-inducible protein HliC. *Photosynthesis Research*, *137*(1), 29–39. https://doi.org/10.1007/s11120-017-0475-7

Skotnicová, P., Staleva-Musto, H., Kuznetsova, V., Bína, D., Konert, M. M., Lu, S., Polívka, T., & Sobotka, R. (2021). Plant LHC-like proteins show robust folding and static non-photochemical quenching. *Nature Communications*, *12*(1), 6890. https://doi.org/10.1038/s41467-021-27155-1

Soo, R. M., Hemp, J., Parks, D. H., Fischer, W. W., & Hugenholtz, P. (2017). On the origins of oxygenic photosynthesis and aerobic respiration in Cyanobacteria. *Science*, *355*(6332), 1436–1440. https://doi.org/10.1126/science.aal3794

Staleva, H., Komenda, J., Shukla, M. K., Šlouf, V., Kaňa, R., Polívka, T., & Sobotka, R. (2015). Mechanism of photoprotection in the cyanobacterial ancestor of plant antenna proteins. *Nature Chemical Biology*, *11*(4), 287–291. https://doi.org/10.1038/nchembio.1755

Tichý, M., Bečková, M., Kopečná, J., Noda, J., Sobotka, R., & Komenda, J. (2016). Strain of Synechocystis PCC 6803 with Aberrant Assembly of Photosystem II Contains Tandem Duplication of a Large Chromosomal Region. *Frontiers in Plant Science*, *7*. https://doi.org/10.3389/fpls.2016.00648

Tribet, C., Audebert, R., & Popot, J.-L. (1996). Amphipols: Polymers that keep membrane proteins soluble in aqueous solutions. *Proceedings of the National Academy of Sciences*, *93*(26), 15047–15050. https://doi.org/10.1073/pnas.93.26.15047

Umena, Y., Kawakami, K., Shen, J.-R., & Kamiya, N. (2011). Crystal structure of oxygen-evolving photosystem II at a resolution of 1.9 Å. *Nature*, *473*(7345), 55–60. https://doi.org/10.1038/nature09913

Verméglio, A. (2001). Photosynthesis: Photobiochemistry and Photobiophysics: *Plant Science*, *161*(6), 1187. https://doi.org/10.1016/S0168-9452(01)00528-3

Wei, X., Su, X., Cao, P., Liu, X., Chang, W., Li, M., Zhang, X., & Liu, Z. (2016). Structure of spinach photosystem II–LHCII supercomplex at 3.2 Å resolution. *Nature*, *534*(7605), 69–74. https://doi.org/10.1038/nature18020

Westphal, S., Heins, L., Soll, J., & Vothknecht, U. C. (2001). *Vipp1* deletion mutant of *Synechocystis*: A connection between bacterial phage shock and thylakoid biogenesis? *Proceedings of the National Academy of Sciences*, *98*(7), 4243–4248. https://doi.org/10.1073/pnas.061501198

Wilson, A., Ajlani, G., Verbavatz, J.-M., Vass, I., Kerfeld, C. A., & Kirilovsky, D. (2006). A Soluble Carotenoid Protein Involved in Phycobilisome-Related Energy Dissipation in Cyanobacteria. *The Plant Cell*, *18*(4), 992–1007. https://doi.org/10.1105/tpc.105.040121

Xiong, J., Fischer, W. M., Inoue, K., Nakahara, M., & Bauer, C. E. (2000). Molecular Evidence for the Early Evolution of Photosynthesis. *Science*, *289*(5485), 1724–1730. https://doi.org/10.1126/science.289.5485.1724

Xu, H., Vavilin, D., Funk, C., & Vermaas, W. (2004). Multiple Deletions of Small Cab-like Proteins in the Cyanobacterium Synechocystis sp. PCC 6803. *Journal of Biological Chemistry*, *279*(27), 27971–27979. https://doi.org/10.1074/jbc.M403307200

Xu, H., Vavilin, D., & Vermaas, W. (2002). The Presence of Chlorophyll b inSynechocystis sp. PCC 6803 Disturbs Tetrapyrrole Biosynthesis and Enhances Chlorophyll Degradation. *Journal of Biological Chemistry*, *277*(45), 42726–42732. https://doi.org/10.1074/jbc.M205237200

Xu, H.-F., Dai, G.-Z., Bai, Y., Shang, J.-L., Zheng, B., Ye, D.-M., Shi, H., Kaplan, A., & Qiu, B.-S. (2022). Coevolution of tandemly repeated *hlips* and RpaB-like transcriptional factor confers desiccation tolerance to subaerial *Nostoc* species. *Proceedings of the National Academy of Sciences*, *119*(42), e2211244119. https://doi.org/10.1073/pnas.2211244119

Yao, D., Kieselbach, T., Komenda, J., Promnares, K., Prieto, M. A. H., Tichy, M., Vermaas, W., & Funk, C. (2007). Localization of the Small CAB-like Proteins in Photosystem II. *Journal of Biological Chemistry*, *282*(1), 267–276. https://doi.org/10.1074/jbc.M605463200